Modeling micro-end-milling operations. Part I: analytical cutting force model

W.Y. Bao, I.N. Tansel *

Mechanical Engineering Department, Florida International University, Center for Engineering and Applied Sciences, 10555 West Flagler Street, Miami, FL 33174, USA

Abstract

A new analytical cutting force model is proposed for micro-end-milling operations. The model calculates the chip thickness by considering the trajectory of the tool tip while the tool rotates and moves ahead continuously. The proposed approach allows the calculation of the cutting forces to be done accurately in typical micro-end-milling operations with very aggressively selected feed per tooth to tool radius (f_t/r) ratio. The difference of the simulated cutting forces between the proposed and conventional models can be experienced when f_t/r is larger than 0.1. The estimated cutting force profile of the proposed model had good agreement with the experimental data. © 2000 Elsevier Science Ltd. All rights reserved.

Keywords: Manufacture; Micro-tools; End-milling; Modeling

1. Introduction

Micro-end-milling operations (MEMO) first found applications in electronics, biomedical and aerospace industries. However, miniaturization of many consumer products and esthetic goals drastically increased MEMO applications in the conventional shop floor. Currently, many state-of-the-art consumer product manufacturers widely use micro-tools of less than 2 mm diameter to prepare the plastic injection molds of their parts. In this paper, a new analytical approach is proposed to estimate the cutting forces more accurately in MEMO.

At first glance, MEMO looks like conventional end-milling operations (CEMO) with only dimensional differences. However, in most of MEMO feed per tooth to tool radius (f_t/r) ratio is selected much larger than CEMO to keep the productivity reasonable. Stress variation on the tiny

* Corresponding author. Tel.: +1-305-348-1932; fax: +1-305-348-3304.
  E-mail address: tanseli@eng.fiu.edu (I.N. Tansel).

Nomenclature

x	feed direction coordinate
y	normal direction coordinate
z_c	the coordinate perpendicular to the x–y plane
t	time (s)
F_t	tangential cutting force (N)
F_r	radial cutting force (N)
F_x	feed direction cutting force (N)
F_y	normal direction cutting force (N)
r	tool radius (inch)
Z	the number of tool teeth
z	the ordinal number of tool teeth
β	tooth helix angle (rad)
n	spindle speed (rpm)
ω	spindle circle speed (1/s)
f	feed rate (ipm)
f_t	feed per tooth (inch)
a	depth of cut (inch)
b	width of cut (inch)
θ	tool cutting angle (rad)
θ_s	integrating start angle (rad)
θ_e	integrating end angle (rad)
h	chip thickness (inch)
λ	leading angle (rad)
α	engagement angle (rad)
φ	workpiece cutting angle (rad)
ψ	tool cutter angle (rad)
F_u	unit force (N)
p	proportional factor
K_m	material coefficient (N/cm^2)

shaft of a micro-tool is much higher than that on a conventional tool. These extreme operating conditions drastically shorten tool life. Less than one hundred inches of tool life is common when hard metals such as stainless steel are machined. If the cutting conditions are not selected properly, micro-tools will be broken in a few seconds. Operators have to select the cutting conditions and monitor the machining operations very carefully since those tools will create unnoticeable sound and vibration. Because of their tiny size, it is very difficult to notice the damaged cutting edges and even the broken shaft. Many hours of machining time could be wasted if the tool failure is not detected in time.

To calculate the cutting forces of CEMO, first analytical expressions were derived [1–3]. To improve the analytical cutting force model, the cutting force coefficient, different cutting con-

ditions, total cutting angle, up and down-milling, symmetric and asymmetric cuts were investigated [4,5]. Later, researchers concentrated on the dynamics of the cutting operation and development of chatter. In those studies, cutting forces were calculated numerically to be able to consider the influence of the present and previous tool vibrations to the uncut chap area [6,7]. To improve the accuracy of simulated cutting forces the use of layers was proposed [8]. The chip removal was kept track of by considering the location of the tool tip and simulated cutting forces successfully generated training cases for neural networks [9]. The available numerical model is capable of estimating the cutting forces in the typical CEMO; however, further work is necessary for MEMO.

In this paper, a new analytical model was developed to represent MEMO. The proposed model can be used to simulate the cutting forces of MEMO with the following objective:

- To simulate the cutting forces more accurately in order to represent the typical MEMO.
- To be able to calculate the important parameters very quickly in MEMO; for example, estimation of maximum cutting forces without simulating the whole tool rotation by using numerical methods.
- To create an analytical model to be able to monitor the tool condition in MEMO with the help of genetic algorithms.
- To estimate the surface quality (including precision and roughness) in face-milling.

In the following sections, the proposed model will be introduced. The experimental setup will be outlined. The differences of both the proposed and conventional models will be discussed. The results and conclusion will be presented.

2. Cutting force modeling of micro-end-milling operations

In this section, the conventional cutting force model will be outlined and a new model will be introduced.

2.1. Conventional cutting force model

Tlusty and Macneil's cutting force model [1] was developed for CEMO in 1997. It was based on the following three assumptions:

2.1.1. Assumption 1
The tangential cutting force is proportional to the cutting area.

$$F_t = K_m bh \tag{1}$$

2.1.2. Assumption 2
The radial cutting force is proportional to the tangential cutting force.

$$F_r = pF_t \tag{2}$$

2.1.3. Assumption 3

The chip thickness can be expressed by the following expression:

$$h = f_t \sin \theta \tag{3}$$

The coordinate system of the model is presented in Fig. 1.

For a certain tool cutting angle θ, the chip thickness h is not a constant but a function of z_c because of the tool helix angle β.

$$dF_t = K h(z_c) dz_c$$

where: $z_c = z_c(\theta)$

$$dz_c = (r/\tan \beta) d\theta$$

The expressions Eq. (1) and Eq. (2) can be rewritten as:

$$dF_t = 2(F_u/f_t) h(\theta) d\theta$$

$$dF_r = 2(F_u/f_t) p h(\theta) d\theta$$

where: $F_u = K_m r f_t / \tan \beta / 2$

The cutting forces of feed and normal directions can be expressed as:

$$dF_x = -dF_t \cos \theta - dF_r \sin \theta = -2(F_u/f_t) h(\theta)(\cos \theta \, d\theta + p \sin \theta \, d\theta) \tag{4}$$

$$dF_y = dF_t \sin \theta - dF_r \cos \theta = 2(F_u/f_t) h(\theta)(\sin \theta \, d\theta - p \cos \theta \, d\theta) \tag{5}$$

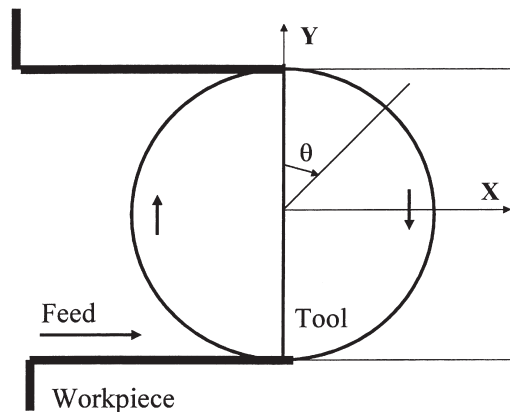Considering the third assumption, the expressions Eq. (4) and Eq. (5) become:

Fig. 1.   Model coordinate system of end-milling operations.

$$dF_x = -2F_u(\sin\theta\cos\theta\,d\theta + p\sin^2\theta\,d\theta)$$

$$dF_y = 2F_u(\sin^2\theta\,d\theta - p\sin\theta\cos\theta\,d\theta)$$

Taking integration, the expressions for the cutting force model were derived as:

$$F_x = -F_u[p(\theta_e-\theta_s)+(\sin^2\theta_e-\sin^2\theta_s)-0.5p(\sin 2\theta_e-\sin 2\theta_s)] \tag{6}$$

$$F_y = F_u[(\theta_e-\theta_s)-p(\sin^2\theta_e-\sin^2\theta_s)-0.5(\sin 2\theta_e-\sin 2\theta_s)] \tag{7}$$

According to the experimental data, the proportional factor p was usually selected as 0.3.
To calculate the cutting forces by using the cutting force model, three computational parameters were introduced.

- Tool cutter angle ψ is defined as:

$$\Psi = 2\pi/Z$$

- Workpiece cutting angle φ is defined as:

$$\varphi = \arccos[(r-a)/r]$$

- Engagement angle α is defined as:

$$\alpha = b\tan\beta/r$$

Most of CEMO can be included in the following three cases.

2.1.4. Case 1
$\alpha\le\varphi$ and $\alpha+\varphi\le\psi$
Up-milling operations

section 1:	$[0, \alpha]$	$\theta_s=0$	$\theta_e=\theta$
section 2:	$[\alpha, \varphi]$	$\theta_s=\theta-\alpha$	$\theta_e=\theta$
section 3:	$[\varphi, \varphi+\alpha]$	$\theta_s=\theta-\alpha$	$\theta_e=\varphi$

Down-milling operations

section 1: $[\pi-\varphi, \pi-\varphi+\alpha]$ $\theta_s=\pi-\varphi$ $\theta_e=\theta$
section 2: $[\pi-\varphi+\alpha, \pi]$ $\theta_s=\theta-\alpha$ $\theta_e=\theta$
section 3: $[\pi, \pi+\alpha]$ $\theta_s=\theta-\alpha$ $\theta_e=\pi$

2.1.5. Case 2
$\alpha\leq\varphi$ and $\alpha+\varphi\leq\psi$
Up-milling operations

section 1: $[0, \varphi]$ $\theta_s=0$ $\theta_e=\theta$
section 2: $[\varphi, \alpha]$ $\theta_s=0$ $\theta_e=\varphi$
section 3: $[\alpha, \varphi+\alpha]$ $\theta_s=\theta-\alpha$ $\theta_e=\varphi$

Down-milling operations

section 1: $[\pi-\varphi, \pi]$ $\theta_s=\pi-\varphi$ $\theta_e=\theta$
section 2: $[\pi, \alpha]$ $\theta_s=\pi-\varphi$ $\theta_e=\pi$
section 3: $[\alpha, \pi+\alpha]$ $\theta_s=\theta-\alpha$ $\theta_e=\pi$

2.1.6. Case 3
$\alpha+\varphi\geq\psi$
Because of overlap, the cutting force of the overlapped part is equal to the sum of the cutting forces of both cutting edges.

The Tlusty and Macneil's model has reasonable assumptions, straightforward derivation and can be easily applied to most of CEMO without tool run-out. It has found many applications in CEMO.

2.2. The proposed cutting force model

In the proposed cutting force model, the chip thickness is calculated by considering the trajectory of the tool tip instead of the third assumption of Tlusty and Macneil's model. In the typical MEMO with a large feed per tooth to tool radius (f_t/r) ratio, the actual chip thickness is very different from that of the conventional model, which are presented in Fig. 2 and Fig. 3. The estimation accuracy can be improved by using the new approach.

In end-milling operations, the trajectory of the tool tip can be written as the following equations.

$$x=\frac{ft}{60}+r\,\sin\left(\omega t-\frac{2\pi z}{Z}\right)\tag{8}$$

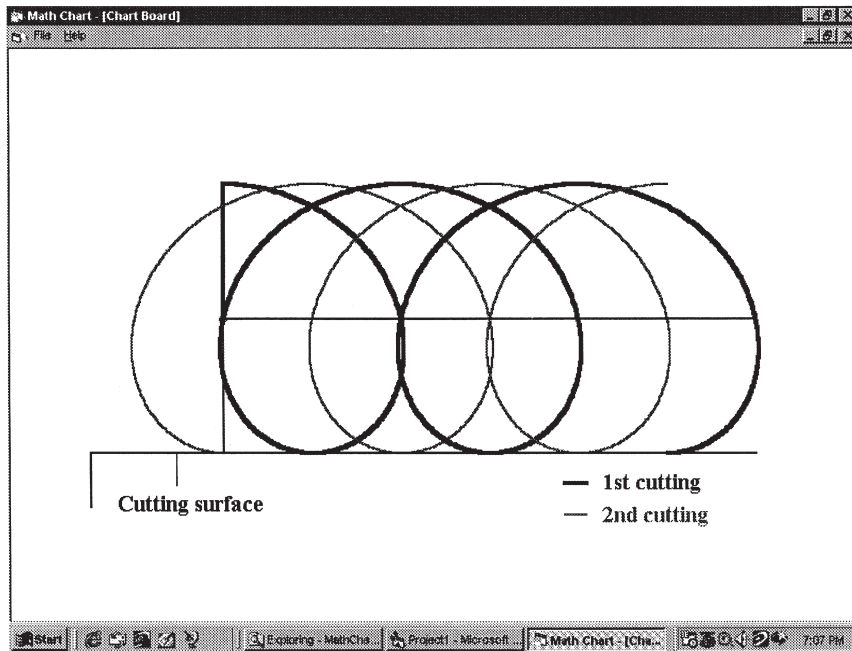$$y=r\,\cos\left(\omega t-\frac{2\pi z}{Z}\right)\tag{9}$$

Fig. 2.   Trajectory of tool tip of micro-end-milling operations.

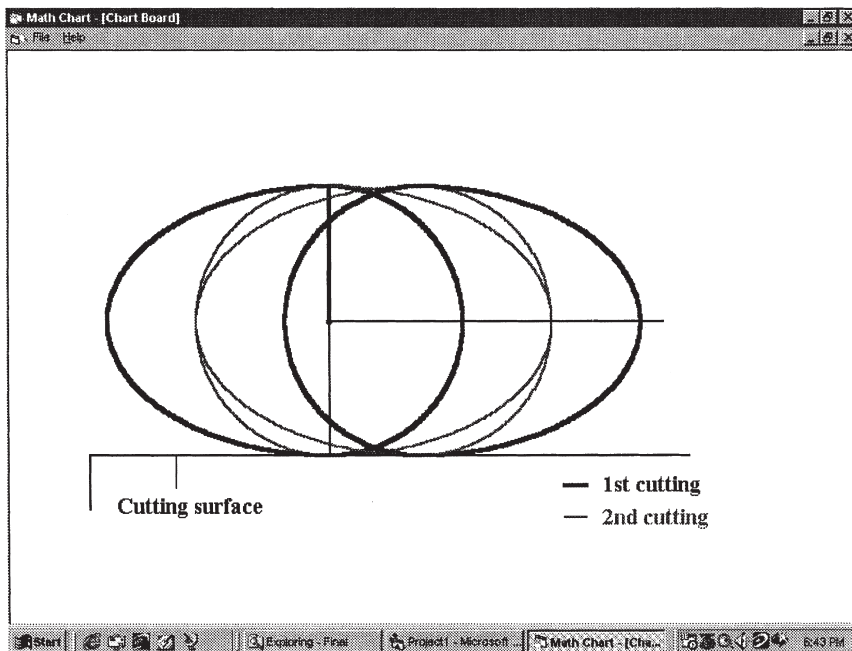Fig. 3.   Trajectory of tool tip of Tlusty and Macneil's model.

The trajectory of tool cutting edges can be written as:

$$\left(x-\frac{ft}{60}\right)\cos\left(\omega t-\frac{2\pi z}{Z}\right)-y\sin\left(\omega t-\frac{2\pi z}{Z}\right)=0 \tag{10}$$

where: $\omega=\dfrac{2\pi n}{60}$

$Z=2$ and $z=0$, 1 for two-flute tools.
$Z=4$ and $z=0$, 1, 2, 3 for four-flute tools.

The intersection of the first cutting edge tip at time t_0 with angle θ_0 and the second cutting edge at time t_1 with angle θ_1 can be solved from Eq. (8) Eq. (9) and Eq. (10).

$$\frac{f}{60\omega}(\omega t_0-\omega t_1)\cos\left(\omega t_1-\frac{2\pi(z+1)}{Z}\right)+r\sin\left(\omega t_0-\omega t_1+\frac{2\pi}{Z}\right)=0$$

Considering geometric conditions, it can be simplified as:

$$\frac{f}{2\pi n}\left(\frac{2\pi}{Z}-\delta\right)\cos\left(\frac{\pi}{2}-\theta_1\right)=r\sin\delta$$

where:

$$\theta_z=\left(1+\frac{4z}{Z}\right)\frac{\pi}{2}-\omega t_z$$

$$\delta=\theta_{z+1}-\theta_z$$

$$\omega t_{z+1}-\omega t_z=\frac{2\pi}{Z}-\delta$$

From the above equation, the computing angle δ can be solved.

$$\delta\approx\frac{f_t\dfrac{\cos\theta}{r}}{1+f_t\dfrac{Z\cos\theta}{2\pi r}}$$

where:

$$f_t=\frac{f}{nZ}$$

$$\theta=\frac{\pi}{2}-\theta_1$$

The computing feed rate is defined as:

$$f_c = \frac{f}{60}(t_1 - t_0)$$

Considering geometric conditions, it can be rewritten as:

$$f_c = \frac{f}{2\pi n}\left(\frac{2\pi}{Z} - \delta\right)$$

Substituting the computing angle δ to the above expression, it becomes:

$$f_c \approx f_t\left(1 - f_t\frac{Z\cos\theta}{2\pi r}\right)$$

Also from geometry, there is:

$$r^2 = H^2 + f_c^2 - 2Hf_c\cos(\pi - \theta_1)$$

The non-cutting edge length H can be solved from the above equation.

$$H = -f_c\sin\theta + \sqrt{r^2 - (f_c\cos\theta)^2}$$

The chip thickness is:

$$h = r - H = r + f_c\sin\theta - \sqrt{r^2 - (f_c\cos\theta)^2}$$

Substituting the computing feed rate f_c to the above expression and simplifying it, the chip thickness expression can be obtained.

$$h \approx f_t\sin\theta - \frac{Z}{2\pi r}f_t^2\sin\theta\cos\theta + \frac{1}{2f}f_t^2\cos^2\theta \tag{11}$$

If the physical meaning of each term of the expression Eq. (11) is evaluated, the first term is a major contributor to the chip thickness. In the conventional model, only this term was considered. The second term presents the difference between up and down-milling. It is a negative variable when θ is changed from 0° to 90° and a positive variable from 90° to 180°. In other words, the chip thickness of down-milling is always bigger than that of up-milling. The third term is an additional chip thickness. In Tlusty and Macneil's model, chip thickness is equal to zero when $\theta = 0°$ or 180°. However, according to expression Eq. (11), the chip thickness is not equal to zero (see Fig. 2).

The cutting force can be derived by substituting the chip thickness expression Eq. (11) into Eq. (4) and Eq. (5).

$$dF_x = -2F_u\left(\sin\theta - \frac{Z}{2\pi r}f_t\sin\theta\cos\theta + \frac{1}{2r}f_t\cos^2\theta\right)(\cos\theta\,d\theta + p\sin\theta\,d\theta)$$

$$dF_y = 2F_u\left(\sin\theta - \frac{Z}{2\pi r}f_t\sin\theta\cos\theta + \frac{1}{2r}f_t\cos^2\theta\right)(\sin\theta\,d\theta - p\cos\theta\,d\theta)$$

Taking integration, the cutting force expressions are:

$$F_x = F_u\left[C_1\frac{f_t}{r}\sin^3\theta + C_2\frac{f_t}{r}\cos^3\theta - \sin^2\theta + \frac{1}{2}p\sin2\theta - \frac{f_t}{r}\sin\theta - p\theta\right]\Bigg|_{\theta_s}^{\theta_e} \tag{12}$$

$$F_y = F_u\left[C_2\frac{f_t}{r}\sin^3\theta - C_1\frac{f_t}{r}\cos^3\theta - p\sin^2\theta - \frac{1}{2}\sin2\theta - p\frac{f_t}{r}\sin\theta + \theta\right]\Bigg|_{\theta_s}^{\theta_e} \tag{13}$$

where:

$$F_u = \frac{K_m r f_t}{2\tan\beta}$$

$$C_1 = \frac{1}{3}\left(1 + p\frac{Z}{\pi}\right)$$

$$C_2 = \frac{1}{3}\left(p - \frac{Z}{\pi}\right)$$

To calculate the cutting force by using the new cutting force model, the leading angle λ has to be considered. It can be derived from expression Eq. (11) by considering $\theta = 0°$.

$$\lambda \approx -\arcsin\left[\frac{f_t}{2r}\left(1 + f_t\frac{Z}{2\pi r}\right)\right]$$

Most of MEMO can be included in the following three cases, where tool cutter angle ψ, workpiece cutting angle φ and engagement angle α have the same definition as the conventional model.

2.2.1. Case 1
$\alpha \leq \varphi + \lambda$ and $\alpha + \varphi + \lambda \leq \psi$
In up-milling operations

section 1:	$[-\lambda, \alpha-\lambda]$	$\theta_s=-\lambda$	$\theta_e=\theta$
section 2:	$[\alpha-\lambda, \varphi]$	$\theta_s=\theta-\alpha$	$\theta_e=\theta$
section 3:	$[\varphi, \varphi+\alpha]$	$\theta_s=\theta-\alpha$	$\theta_e=\varphi$

In down-milling operations

section 1:	$[\pi-\varphi, \pi-\varphi+\alpha]$	$\theta_s=\pi-\varphi$	$\theta_e=\theta$
section 2:	$[\pi-\varphi+\alpha, \pi+\lambda]$	$\theta s=\theta-\alpha$	$\theta_e=\theta$
section 3:	$[\pi+\lambda, \pi+\lambda+\alpha]$	$\theta_s=\theta-\alpha$	$\theta_e=\pi+\lambda$

2.2.2. Case 2
$\alpha \geq \varphi+\lambda$ and $\alpha+\varphi+\lambda \leq \psi$
In up-milling operations

section 1:	$[-\lambda, \varphi]$	$\theta_s=-\lambda$	$\theta_e=\theta$
section 2:	$[\varphi, \alpha-\lambda]$	$\theta_s=-\lambda$	$\theta_e=\varphi$
section 3:	$[\alpha-\lambda, \varphi+\alpha]$	$\theta_s=\theta-\alpha$	$\theta_e=\varphi$

In down-milling operations

section 1:	$[\pi-\varphi, \pi+\lambda]$	$\theta_s=\pi-\varphi$	$\theta_e=\theta$
section 2:	$[\pi+\lambda, \pi-\varphi+\alpha]$	$\theta_s=\pi-\varphi$	$\theta_e=\pi+\lambda$
section 3:	$[\pi-\varphi+\alpha, \pi+\lambda+\alpha]$	$\theta_s=\theta-\alpha$	$\theta_e=\pi+\lambda$

2.2.3. Case 3
$\alpha+\varphi+\lambda \geq \psi$
Because of overlapping, the cutting force of the overlapped part is equal to the sum of the cutting forces of both cutting edges.

3. Experimental setup

More than 800 cutting experiments of MEMO were performed in the Mechatronics Lab of the Mechanical Engineering Department of Florida International University and the Engineering Prototype Center of Radio Technology Division of Motorola Inc., and more than 200 megabytes of cutting force data were recorded. The experimental contents are listed in Table 1.

The typical experimental setup is presented in Fig. 4. Three different types of milling machines were used in the experiments. The workpiece was set on a dynamometer that was installed on the table of the machine tool. Two components of the cutting force were recorded by using a digital oscilloscope through a charge amplifier. The experimental equipment is listed in Table 2.

Table 1
Experimental contents

|	
Tool types:	Two-flute and four-flute micro-end-mills
Tool diameters (inch):	5/1000, 20/1000, 30/1000, 1/32, 1/16, 1/8
Tool materials:	High-speed steel (HSS), carbide
Workpiece materials:	Metal materials: Aluminum, Copper, Mild steel, NAK-55 steel and 3DP materialsNon-metal materials: EDM POCO-3 and EDM POCO-C3 graphite
Working conditions:	Slot and 50% overlapped down-milling with different spindle speed, feed rate and width of cut
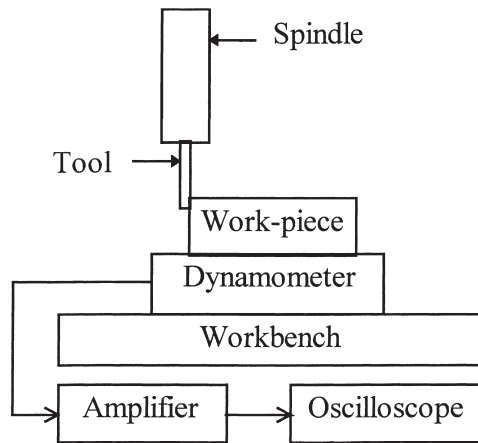
Fig. 4.   Experiment setup.

Table 2
Experimental equipment

Machine tools:	Bridgeport series I 3,000 rpm milling machine
	Fadal 3-axis 15,000 rpm CNC machine
	Fadal 5-axis 50,000 rpm CNC machine
Data acquisition:	Nicolet 310 digital oscilloscope
	Nicolet integra model 10 digital oscilloscope
Cutting force measurement:	Kistler 9257B 3-component piezoelectric dynamometer
	Kistler 3-channel charge amplifier

4. Results and discussion

In this section, the accuracy of the simulated cutting force profile of the proposed model is evaluated. The differences between the proposed and conventional models are discussed. Their variation of the accuracy of the cutting force estimations at different f_t/r ratios are presented.

4.1. Verification of the proposed model

The proposed analytical cutting force model was presented as expressions Eq. (12) and Eq. (13). The model used eight parameters and one coefficient to represent the cutting forces of MEMO and CEMO without tool runout.

- Three working condition variables: spindle speed (n), feed rate (f) and width of cut (b).
- Two cutting condition variables: tool cutting entry and exit angle, which presents depth of cut (a), and up- and down-milling.
- Three tool geometry variables: tool diameter ($2r$), helix angle (β) and the numbers of tool flutes (N).
- Material coefficient (K_m) is related to the tool and workpiece materials, which could be determined by a few experiments.

The model has been tested on the experimental data of hundreds of MEMO cases and very good agreement has been observed between the theoretical and experimental results. The average error between computational and experimental maximum cutting forces was around 10%. The results of eight test cases with different workpiece materials and operating conditions are presented in Table 3.

In Table 3, the data were collected from two designed experimental sets. First a two-flute carbide end-mill with 1/16″ diameter cut on a NAK-55 steel workpiece with four different operating conditions (from case 1 to 4). The collected cutting force data of four different operating conditions were used to decide the cutting force coefficient of an analytical model. The model was optimized by using a genetic algorithm program according to minimum average error between the computing cutting forces of the analytical model and the cutting force data collected from the four experimental cases. From Table 3, it is easily understood when the analytical model was chosen very close to the case 2 conditions it had the best results to represent the cutting forces of those four machining operations. The other experiments, a two-flute carbide end-mill with

Table 3
Error between computational and experimental maximum cutting forces

Test No.	End-mill (two-flute)	Workpiece material	Spindle speed (rpm)	Feed rate (ipm)	Width of cut (inch)	Depth of cut (inch)	Error of cutting force between the simulation and test
1	1/16″ carbide	NAK-55 steel	15,000	5.0	1/16	1/32	28.1%
2	1/16″ carbide	NAK-55 steel	15,000	7.5	1/16	1/32	0.0%
3	1/16″ carbide	NAK-55 steel	15,000	5.0	1/32	1/32	15.8%
4	1/16″ carbide	NAK-55 steel	15,000	7.5	1/32	1/32	10.6%
5	1/16″ carbide	Aluminum	32,000	32	0.02	1/32	4.6%
6	1/16″ carbide	Aluminum	32,000	48	0.02	1/32	13.0%
7	1/16″ carbide	Aluminum	50,000	50	0.02	1/32	6.3%
8	1/16″ carbide	Aluminum	50,000	75	0.02	1/32	0.0%
Average							9.8%

1/16″ diameter machined an aluminum workpiece with four different operating conditions (from case 5 to 8). The analytical cutting force model for aluminum and carbide end-mill cases was optimal according to the same method discussed above.

4.2. Simulation of micro-end-milling operations by using the proposed model

The comparisons of two test cases between the simulated and experimental cutting force profiles are presented in Figs 5 to 10.

A two-flute 1/8″-diameter carbide end-mill was used to cut a steel workpiece. Down-milling operations were performed with the cutting conditions of 2,000 rpm spindle speed, 1 ipm feed rate, 1/16″ width of cut and 1/16″ depth of cut. The simulated and experimental feed and normal direction cutting force profiles are presented in Fig. 5 and Fig. 6, and a comparison of them is made in Fig. 7.

A two-flute 1/16″-diameter carbide end-mill machined an aluminum workpiece with down-milling operations. The cutting conditions were 32,000 rpm spindle speed, 32 ipm feed rate, 0.020″ width of cut and 1/32″ depth of cut. The simulated and experimental feed and normal direction cutting force profiles are presented in Fig. 8 and Fig. 9, and a comparison of them is made in Fig. 10.

The difference between the estimated and experimental maximum cutting forces of the two presented cases was less than 5% (0.6% error in the steel workpiece case, and 4.6% error in the aluminum workpiece case).

4.3. Comparison of the proposed model with the conventional model and numerical approaches

If $f_t/r \ll 1$, the proposed model can be simplified to the following expressions:

$$F_x = F_u \left[-\sin^2 \theta + \frac{1}{2} p \sin 2\theta - p\theta \right] \Bigg|_{\theta_s}^{\theta_e} \tag{14}$$
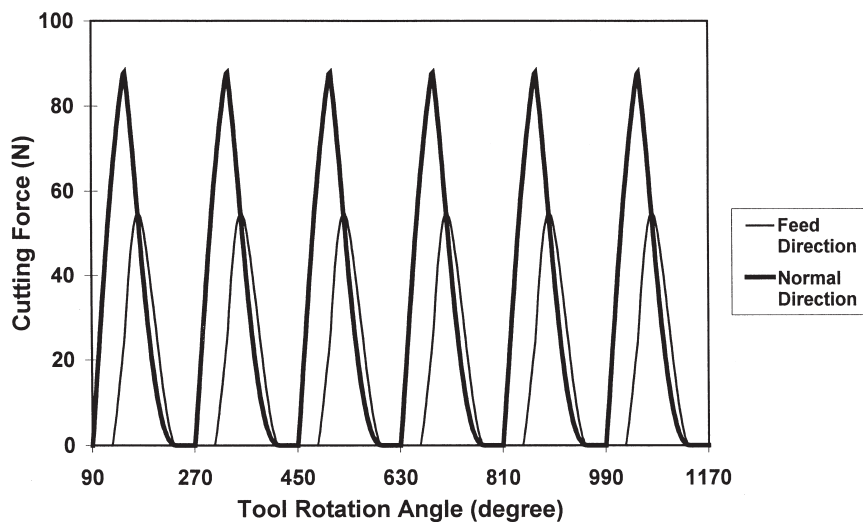

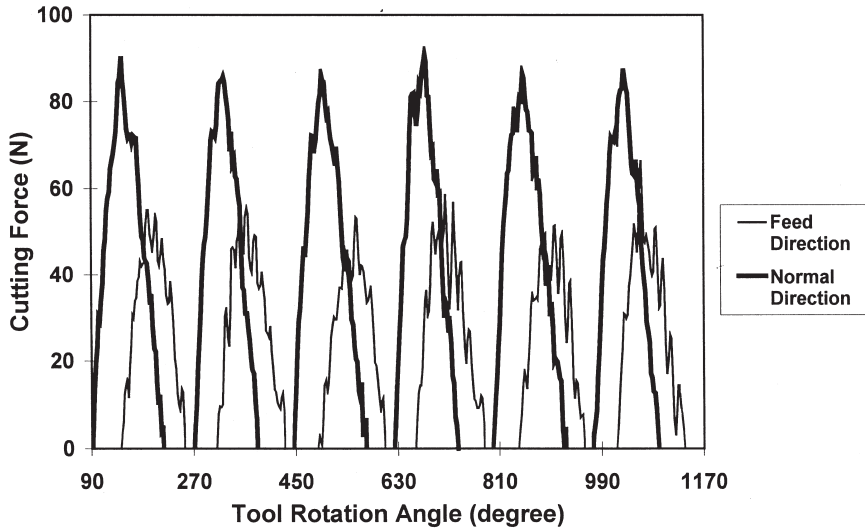Fig. 5.   Simulated feed and normal direction cutting force profiles of MEMO (steel workpiece).

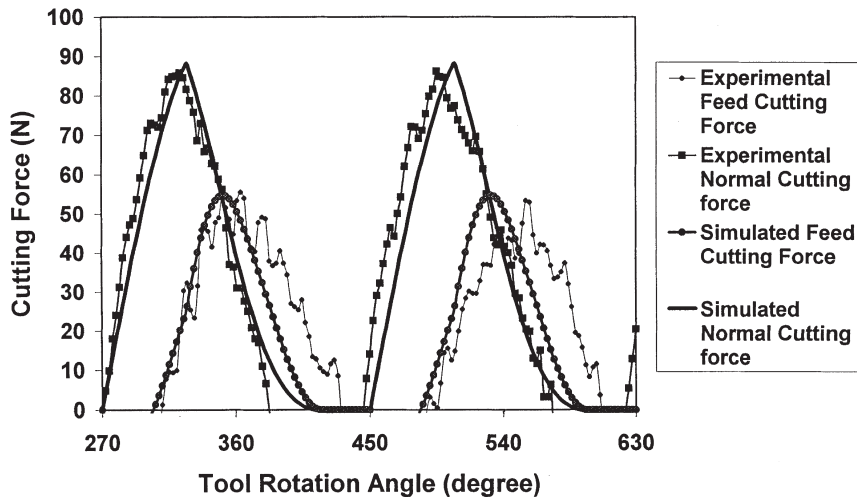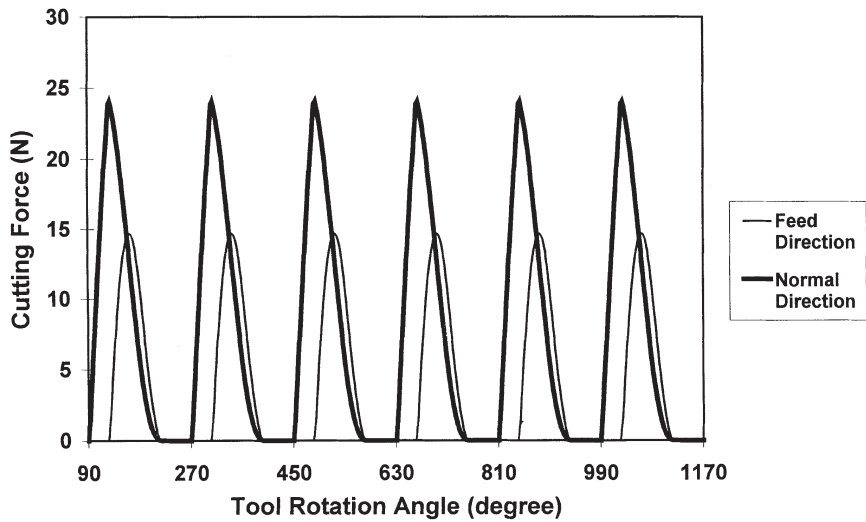Fig. 6.   Experimental feed and normal direction cutting force profiles of MEMO (steel workpiece).

Fig. 7.   Comparison of simulated and experimental cutting force of MEMO (steel workpiece).

$$F_y = F_u \left[-p \sin^2 \theta - \frac{1}{2} \sin 2\theta + \theta \right]\Bigg|_{\theta_s}^{\theta_e} \tag{15}$$

Expressions Eq. (14) and Eq. (15) are exactly the same as the cutting force expressions in Tlusty and Macneil's model (expressions (6) and (7)). The conventional model is only a special

Fig. 8.   Simulated feed and normal direction cutting force profiles of MEMO (aluminum workpiece).
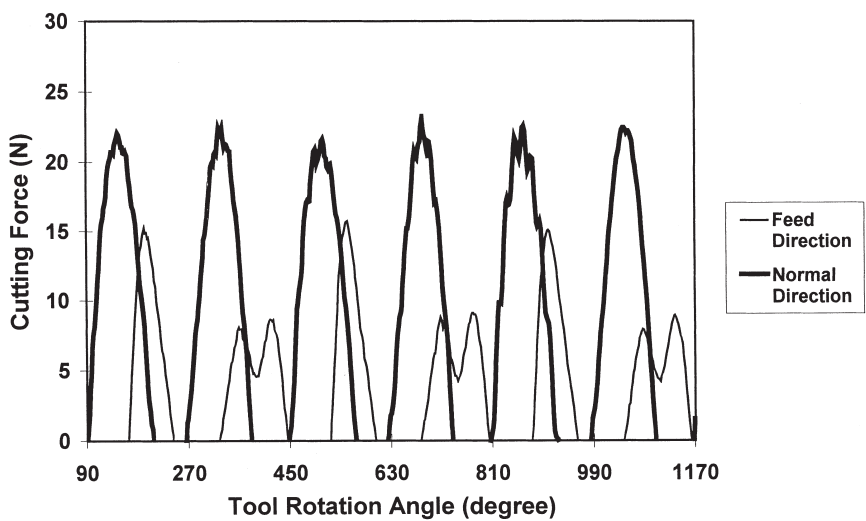

Fig. 9.   Experimental feed and normal direction cutting force profiles of MEMO (aluminum workpiece).

case of the proposed model when the feed per tooth to tool radius (f_t/r) ratio is small enough to be neglected. It can be directly derived from the proposed model by simply letting $f_t/r=0$.

In the proposed approach, the chip thickness expression Eq. (11), which was derived directly from the tool tip trajectory Eq. (8) and Eq. (9) and tool cutting edge trajectory Eq. (10), verifies the third assumption of Tlusty and Macneil's model (expression (3)) when $f_t/r \ll 1$. It not only proves the third assumption of Tlusty and Macneil's model theoretically but also presents its limitation.

Tlusty and Macneil's model has an unnegligible error of cutting force estimation when the f_t/r
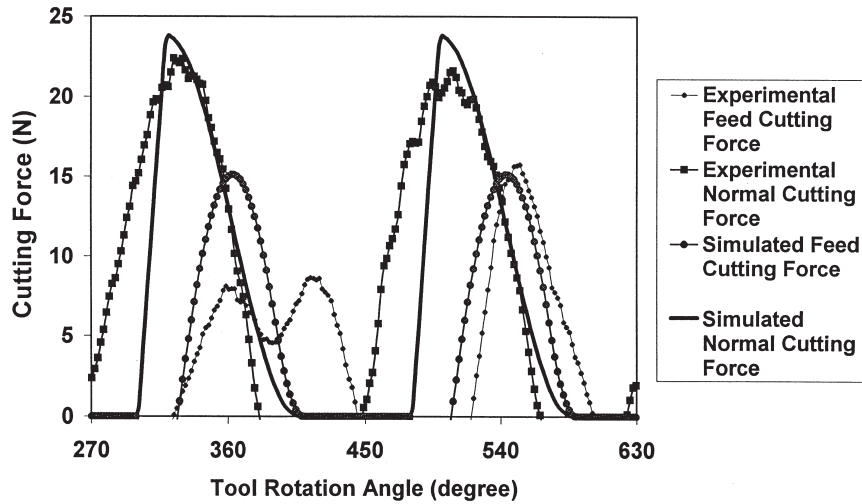
Fig. 10. Comparison of simulated and experimental cutting force of MEMO (aluminum workpiece).

ratio becomes larger. The error depends on the f_t/r ratios. To evaluate the limitation of Tlusty and Macneil's model, the difference of the cutting forces between the proposed and conventional models was investigated at different f_t/r ratios and the results are presented in Fig. 11 and Fig. 12. According to Fig. 11 and Fig. 12, the error of the maximum cutting force estimation by using Tlusty and Macneil's model is larger than 15% when f_t/r is larger than 0.1. In other words, if f_t/r is less than 0.1, both models have very close results. The conventional model could be used to simulate MEMO and estimate the cutting forces with less than 15% error.

The proposed approach is capable of estimating the cutting forces much faster than the numerical approaches that calculate the cutting forces by considering the rotation of tool tip with small
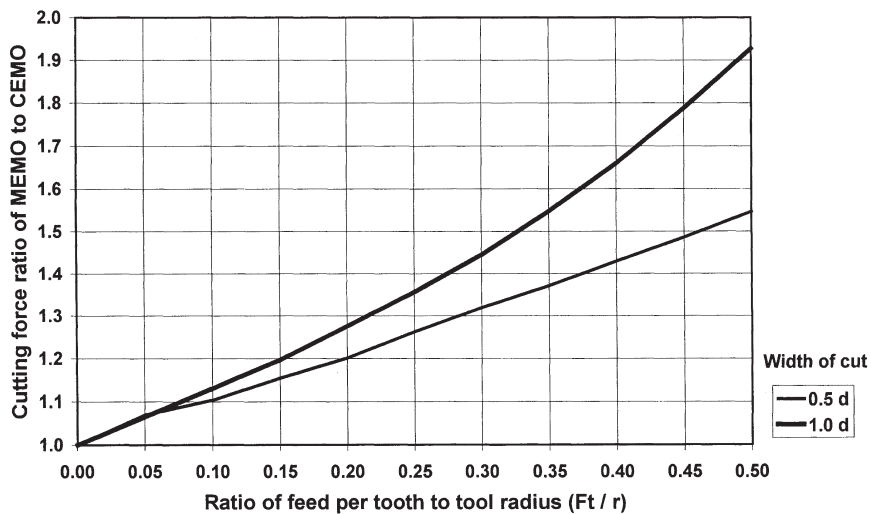

Fig. 11. Difference of feed direction cutting force between MEMO and CEMO models.
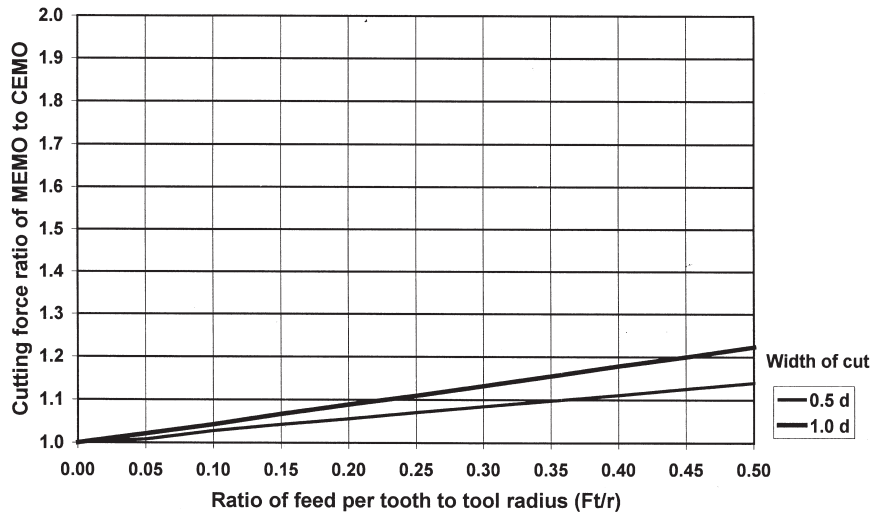
Fig. 12.   Difference of normal direction cutting force between MEMO and CEMO models.

steps and geometry. The proposed expressions can be used to estimate the operating conditions and cutting force coefficients of each cutting edge by using a fast optimization method from the monitored cutting force data. If these estimations are performed in almost real time by using fast optimization algorithms such as genetic algorithms, the tool condition can be evaluated by inspecting the coefficients [10]. The increasing cutting coefficient of a cutting edge indicates tool wear [11]. When the cutting force coefficient of a cutting edge becomes zero while the others exist, that tool tip is broken.

5. Conclusion

A new analytical cutting force model is proposed for MEMO. The validity of the model is proven by comparing it with the existing analytical model and experimental data. The average error between the computational and experimental cutting force was around 10%.

Compared to the conventional model, the proposed model estimates the cutting force more accurately in the typical MEMO with an aggressive feed per tooth to tool radius (f_t/r) ratio. The conventional analytical model (Tlusty and Macneil's model) can be derived from the proposed model by considering that the f_t/r ratio is equal to zero. The difference of the cutting force estimations between the proposed and conventional models is less than 15% if f_t/r is less than 0.1.

Expressions for the maximum cutting force, variation of the cutting force in one complete rotation, surface quality and many other characteristics of the cutting force components can be derived from the proposed cutting force model. By using these expressions these variables can be calculated very quickly compared to numerical simulation programs that calculate the cutting forces by evaluating the location of tool tip at the present and previous rotations. The results can be presented with charts to allow machining operators to easily select the cutting conditions.

Using a fast optimization technique such as genetic algorithms, the proposed model can be

used to estimate the operating conditions and cutting force coefficients of each cutting edge from the monitored cutting force data. Tool breakage and wear can be estimated by inspecting the estimated cutting force coefficients.

References

[1] J. Tlusty, P. Macneil, Dynamics of cutting forces in end milling, Annals of the CIRP 24 (1) (1975) 21–25.

[2] P.E. Gygax, Dynamics of single-tooth milling, IWF/ETH Zurich, Annals of the CIRP 28 (1) (1979) 65–70.

[3] W.A. Kline, R.E. DeVor, The effect of cutter runout on cutting geometry and forces in end milling, Int, J. of Mach. Tool Des. and Res. 23 (1983) 123–148.

[4] G. Yucesan, A.E. Bayoumi, L.A. Kendall, An analytic cutting force model for milling, Transactions of the North American Manufacturing Research Institution of SME 1990, May 1990, 137-145.

[5] K. Jemlelniak, Modelling of dynamic cutting coefficients in three-dimensional cutting, International Journal of Machine Tools and Manufacture 32 (4) (1992) 509–519.

[6] J. Tlusty, F. Ismail, Special aspects of chatter in milling, Trans. of ASME, Journal of Eng. for Ind. 105 (1983) 24–32.

[7] F. Ismail, A. Bastami, Improving stability of slender end mills against chatter, Trans. of ASME, Jour. of Eng. for Ind. 108 (1986) 264–268.

[8] I.N. Tansel, C. McLaughlin, M. Clements, Identification of tool breakage in milling operations by using on-line tooth modeling, in: M.H. Hamza (Ed.), IASTED International Symposium on Robotics and Manufacturing ACTA Press, 1989, pp. 244–248.

[9] I.N. Tansel, C. McLaughlin, Detection of tool breakage in milling operations: Part 2 - The neural network approach, International Journal of Machine Tools and Manufacturing 33 (4) (1993) 545–558.

[10] I.N. Tansel, W.Y. Bao, B. Tansel, B. Shisler, D. Smith, J. Murray, Identification of cutting conditions by using an analytical model and genetic algorithms for micro-end-milling operations, smart engineering system design: Neural networks, fuzzy logic, rough sets and evolutionary programming, in: Intelligent Engineering Systems Through Artificial Neural Networks, vol. 8, ASME Press, 1998, pp. 779–784.

[11] I.N. Tansel, W.Y. Bao, N. Mahendrakar, S.Y. Yang, B. Shisler, D. Smith, J. Murray, Tool wear monitoring in micro-end-milling operations by using genetic algorithms. Accepted for the Artificial Neural Networks in Engineering (ANNIE'99) Conference, 1999.